PNAS RESEARCH ARTICLE | MICROBIOLOGY

The HUSH epigenetic repressor complex silences PML nuclear body-associated HSV-1 quiescent genomes

Simon Roubille[a,1], Tristan Escure[a,1], Franceline Juillard[a,b,1], Armelle Corpet[a,c,1], Rémi Néplaz[a], Olivier Binda[a,d], Coline Seurre[a], Mathilde Gonin[a], Stuart Bloor[e], Camille Cohen[a,f], Pascale Texier[a], Oscar Haigh[g], Olivier Pascual[h], Yonatan Ganor[i], Frédérique Magdinier[j], Marc Labetoulle[g,k,l], Paul J. Lehner[e], and Patrick Lomonte[a,2]

Affiliations are included on p. 11.

Edited by Thomas Shenk, Princeton University, Princeton, NJ; received June 25, 2024; accepted October 21, 2024

Herpes simplex virus 1 (HSV-1) latently infected neurons display diverse patterns in the distribution of the viral genomes within the nucleus. A key pattern involves quiescent HSV-1 genomes sequestered in promyelocytic leukemia nuclear bodies (PML NBs) forming viral DNA-containing PML-NBs (vDCP NBs). Using a cellular model that replicates vDCP NB formation, we previously demonstrated that these viral genomes are chromatinized with the H3.3 histone variant modified on its lysine 9 by trimethylation (H3.3K9me3), a mark associated with transcriptional repression. Here, we identify the HUSH complex and its effectors, SETDB1 and MORC2, as crucial for the acquisition of H3K9me3 on PML NB-associated HSV-1 and the maintenance of HSV-1 transcriptional repression. ChIP-seq analyses show H3K9me3 association with the entire viral genome. Inactivating the HUSH–SETDB1–MORC2 complex before infection significantly reduces H3K9me3 on the viral genome, with minimal impact on the cellular genome, aside from expected changes in LINE-1 retroelements. Depletion of HUSH, SETDB1, or MORC2 alleviates HSV-1 repression in infected primary human fibroblasts and human induced pluripotent stem cell–derived sensory neurons (hiPSDN). We found that the viral protein ICP0 induces MORC2 degradation via the proteasome machinery. This process is concurrent with ICP0 and MORC2 depletion capability to reactivate silenced HSV-1 in hiPSDN. Overall, our findings underscore the robust antiviral function of the HUSH–SETDB1–MORC2 repressor complex against a herpesvirus by modulating chromatin marks linked to repression, thus presenting promising avenues for anti-herpesvirus therapeutic strategies.

Microbiology | epigenetics | HUSH

Significance

Herpes simplex virus 1 (HSV-1) is a major human pathogen, which remains latent in the trigeminal ganglianeurons of the infected individuals. Its reactivation is characterized by a variety of clinical symptoms the most severe ones being keratitis and herpesvirus encephalitis. The colonization of the CNS by the virus during the individual life is a well-known fact, but the pathophysiological effects on neuron homeostasis are still underestimated. It is thus paramount to understand the molecular mechanisms that control HSV-1 latency and maintain the virus in a pseudosilent state. Here, we show that the HUSH–SETDB1–MORC2 axis plays an essential role in repressing the HSV-1 genome which opens up different strategies to treat herpesvirus-associated pathologies.

The establishment of latent herpes simplex virus 1 (HSV-1) infection involves a complex interplay of cellular and molecular events. At the epigenetic level, this requires the viral chromatinization and interaction of latent episomal viral genomes with their nuclear environment (1, 2). Promyelocytic leukemia nuclear bodies (PML NBs also named ND10) are nuclear membrane-less organelles involved in the transcriptional control of HSV-1 latent genomes (2, 3). The protein composition of PML NBs is highly dynamic due to their phase separation properties (4). Following HSV-1 genomes nuclear entry, PML NBs sequester HSV-1 genomes (2, 5, 6) and control the acquisition of repressive histone marks of PML NB-associated HSV-1 genomes (also named viral DNA-containing PML NBs, vDCP NBs, or ND10-like) (7). VDCP NBs, a major hallmark of HSV-1 latently infected neurons, are characterized by their ability to maintain latent HSV-1 genomes in a transcriptionally inactive, but reversible, state of quiescence (2, 3). PML NBs, and by extension vDCP NBs, are disrupted by infected cell protein 0 (ICP0), a virus-encoded ubiquitin E3 ligase, which counteracts the intrinsic host antiviral defense mechanisms and is essential for the initiation of HSV-1 lytic reactivation and replication from latency (7–11). Di- and trimethylation of lysine 9 of histone H3 (H3K9me3) marks repressive heterochromatin in general and is with H3K27me3 associated with repressed latent HSV-1 genomes (1, 7, 12–14), but the cellular factor(s) involved in the establishment and maintenance of HSV-1 latency remain poorly defined (15, 16).

Three methyltransferases are responsible for the deposition of H3K9me3 in mammalian cells: SUV39H1/2 and ESET/SETDB1 (hereafter named SETDB1) (17). In mouse cells, SETDB1 is a major constituent of PML NBs (18). SETDB1 is responsible for silencing proviral elements in ESC cells (19) and associates with the human cytomegalovirus genome in CD34+ latently infected cells (20). We identified HUSH (Human Silencing Hub) as an epigenetic repressor complex which silences integrated retroelements (21, 22). These include retroviruses, such as latent HIV (21), as well as retrotransposons (23, 24). HUSH

The authors declare no competing interest.

This article is a PNAS Direct Submission.

[1]S.R., T.E., F.J., and A.C. contributed equally to this work.

[2]To whom correspondence may be addressed. Email: patrick.lomonte@univ-lyon1.fr.

This article contains supporting information online at https://www.pnas.org/lookup/suppl/doi:10.1073/pnas.2412258121/-/DCSupplemental.

Published November 26, 2024.

also suppresses recombinant adeno-associated virus (rAAV) (25) and normally integrated viruses that have been engineered to remain unintegrated, such as murine leukemia virus (MLV) (26). HUSH made up of three core components, TASOR (transgene activation suppressor), MPP8 (M-phase phosphoprotein 8), and Periphilin (PPHLN1) and recruits two effector proteins: The SETDB1 methyltransferase deposits repressive H3K9me3 heterochromatin (21), and the MORC2 (microrchidia CW-type zinc-finger) ATP-dependent chromatin remodeler, which compacts chromatin (27), and is frequently mutated in Charcot–Marie–Tooth disease CMT2Z patients (28).

Here, we investigate the role of SETDB1 and the HUSH complex in the regulation of PML NB-associated quiescent HSV-1, an unintegrated herpesvirus genome. We find that HUSH, SETDB1, and MORC2 participate to an epigenetic environment which allows the establishment and maintenance of HSV-1 repression in vDCP NBs in primary human fibroblasts as well as sensory neurons derived from human induced pluripotent stem cells (hiPSDN), the main cells supporting HSV-1 latency.

Results

SETDB1 Is a Major Determinant of vDCP NBs. To understand how the HSV-1 viral genome is maintained in the quiescent state, we initially infected primary human fibroblast cells (hFC) with a quiescence-prone HSV-1 (lqHSV-1) mutant (7), a model system we previously showed to reproduce the formation of vDCP NBs, as seen in trigeminal neurons of latently infected mice and human (2, 3). Proteins of the H3.3 histone chaperone complex HIRA bind naked nonchromatinized DNA (29) and are recruited to vDCP NBs where they bind the incoming HSV-1 genome (7). LqHSV-1 genome chromatinization with H3.3 by the HIRA complex and PML protein results in K9 trimethylation of the H3.3 histone variant (7).

UBN1 coprecipitates with a histone H3K9 methyltransferase activity (30), and SETDB1 is a component of PML NBs in mouse cells (18). Therefore, we investigated whether SETDB1 could play a role in HSV-1-dependent silencing. SETDB1 was readily detected in PML NBs of noninfected (NI) and infected (I) hFC (*SI Appendix*, Fig. S1*A*), remaining associated with PML NBs in lqHSV-1 infected cells for at least 7 d postinfection (dpi) (*SI Appendix*, Fig. S1*A*) and colocalizing with lqHSV-1 genomes in all infected cells (*SI Appendix*, Fig. S1*B*). These data suggest that SETDB1 and its partner proteins could be putative molecular determinants in the epigenetic regulation of PML NB-associated quiescent HSV-1 genomes.

The HUSH Complex and MORC2 Accumulate in vDCP NBs Following HSV-1 Quiescent Infection. Given the close functional interaction between SETDB1, the HUSH complex, and MORC2, we investigated their presence in PML NBs and vDCP NBs in NI and infected cells. Proteins detected by IF-FISH, including endogenous SETDB1 and MPP8, but excluding TASOR, colocalized with vDCP NBs in quiescently infected hFC (Fig. 1) and were present in the same structures as exemplified by the concomitant detection of SETDB1 and MPP8 colocalizing with viral genomes (*SI Appendix*, Fig. S1*C*). Unlike endogenous SETDB1 (*SI Appendix*, Fig. S1) and overexpressed proteins (except for TASOR), none of the endogenous core HUSH complex proteins or MORC2 could be detected in PML NBs in NI hFC (Fig. 1 and *SI Appendix*, Fig. S2). We performed ChIP analysis at 24 h pi to determine whether the proteins of the HUSH complex and its effectors were recruited on the HSV-1 genome. Multiple loci (promoter and/or coding region (CDS), see *Materials and Methods* for details) within the viral genome were analyzed, which together represent all classes of lytic and latent genes (Fig. 2*A*). Only the antibody against endogenous MPP8 gave reliable results by ChIP and showed a strong interaction between MPP8 and all viral loci (Fig. 2*B* and *SI Appendix*, Fig. S4*A* for interactions of endogenous MPP8 with representative cellular loci in hFC). Ectopic tagged HUSH components and their effectors could also be found enriched on the quiescent viral genome (*SI Appendix*, Fig. S3). We have previously demonstrated that the interaction of chromatin modulators including the H3.3 chaperone proteins HIRA, UBN1, DAXX, and ATRX across the lqHSV-1 genome is a specific feature of the quiescent state corresponding to the association of HSV-1 genomes with PML NBs (7). Together, these data suggest a role for the HUSH complex, together with SETDB1 and MORC2, in the epigenetic regulation of PML NB-associated quiescent HSV-1 genomes.

PML and the HUSH–SETDB1–MORC2 Repressor Complex Are Independent for Their Interaction with lqHSV-1. In order to investigate the interaction and/or colocalization of HSV-1 genomes with HUSH–SETDB1–MORC2 proteins in the absence of PML, PML-depleted hFC (7) were infected with lqHSV-1, and ChIP-qPCR or FISH-IF were conducted. The ChIP results show that depleting PML before infection does not affect the interaction between endogenous MPP8 with the lqHSV-1 genomes (*SI Appendix*, Fig. S4 *B–D*). Quantification of FISH-IF data reveals that the depletion of PML does not decrease the colocalization of endogenous MPP8 with lqHSV-1 genomes (Fig. 2 *C–E*). Similarly, individual depletion of HUSH–SETDB1–MORC2 proteins does not impact the formation of vDCP NBs as monitored by the colocalization of PML or ATRX, one of the major components of PML NBs, with lqHSV-1 (Fig. 2*F* and *SI Appendix*, Fig. S5 *A–C*). These findings suggest that, while ultimately all cellular components are present in the vDCP NBs, the interaction between lqHSV-1 genomes with PML/PML NBs and the HUSH–SETDB1–MORC2 repressor complex may occur independently of each other.

The HUSH Complex with SETDB1 and MORC2 Controls the Deposition of Repressive Histone Marks on the Quiescent PML NB-Associated HSV-1 Genome. To further investigate the role of HUSH components in the acquisition of the H3K9me3 mark on the lqHSV-1 genome, we took a knock down approach, transducing hFC with previously validated and specific shRNAs (21, 27) (Fig. 3*A*) and verified their efficiency at the protein level (Fig. 3 *B–F*). With the unexpected exception of TASOR, depletion of the proteins induced a significant decrease of the H3K9me3 mark across the quiescent viral genome (Fig. 3*G* and expanded data in *SI Appendix*, Fig. S6). A siRNA targeting SETDB1 gave similar results (*SI Appendix*, Fig. S7). The reduction in H3K9me3 levels on the lqHSV-1 genome could not be linked to a general decrease of the total H3K9me3 mark in the shRNA-treated cells, as observed in Western blotting (*SI Appendix*, Fig. S8*A*). Moreover, the deficit in H3K9me3 on the lqHSV-1 genome did not stem from a general decrease in histone H3 binding, as indicated by ChIP analyses (*SI Appendix*, Fig. S8 *B–F*). In contrast to SETDB1, SUV39H1, another H3K9me3 methyltransferase (17), was not detectable in the PML NBs in both noninfected and infected hFC (*SI Appendix*, Fig. S9*A*). Depletion of SUV39H1 via specific siRNA did not diminish the levels of H3K9me3 associated with the lqHSV-1 genome (*SI Appendix*, Fig. S9 *B–E*).

Next, we conducted ChIP sequencing (ChIP-seq) in infected cells to comprehensively examine the deposition of the H3K9me3 mark on both the lqHSV-1 and cellular genomes. Our findings confirmed the presence of this mark across the entire viral genome

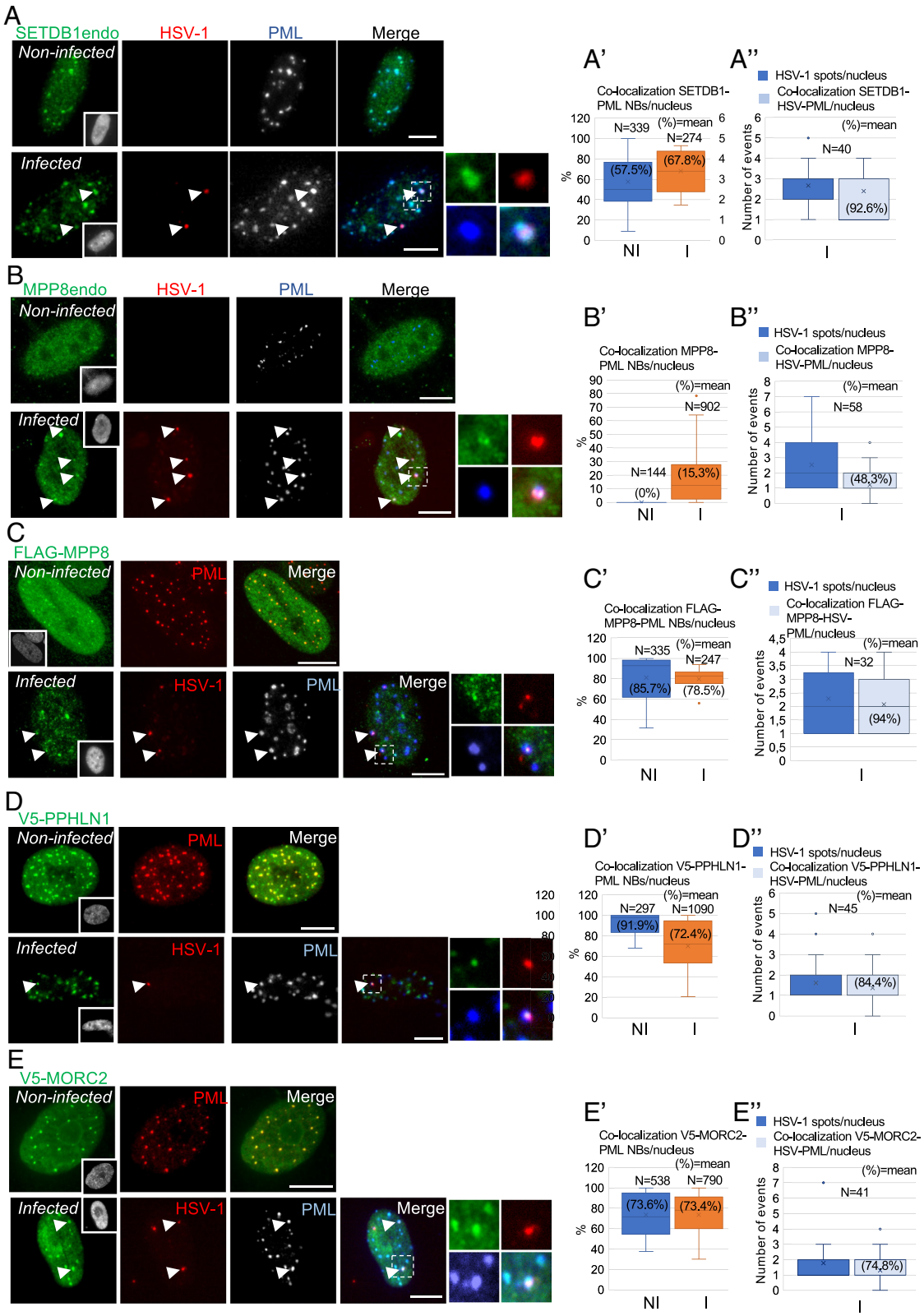

Fig. 1. Detection of proteins of the HUSH–SETDB1–MORC2 entity in vDCP NBs. FISH-IF to detect proteins of the HUSH–SETDB1–MORC2 (green) entity and PML (blue/gray) together with HSH-1 genomes. hFC were infected or not with lqHSV-1 (m.o.i.= 3, 100% of cells infected) and harvested at 4 dpi to perform immuno-FISH. Endogenous SETDB1 and MPP8 were readily detectable with native antibodies supporting the FISH procedure. All other proteins were detected through the expression of an ectopic tagged version. FLAG-MPP8 was also detected as a control for the other HUSH complex components. Insets represent nuclei. Zooms point out vDCP NBs. (*A–E*) Detection of endogenous SETDB1, endogenous MPP8, FLAG tagged MPP8, v5 tagged periphilin (PPHLN1), and v5 tagged MORC2, respectively, in noninfected (NI) and infected (I) cells. (Scale bars, 5 μm.) (*A'–E'*) Quantification of the colocalization of the protein with PML NBs for the respective samples in NI and I cells. Means are indicated in the graphs. (*A''–E''*), Quantification of the average number of HSV-1 spots per nucleus (dark blue) and of the colocalization of the protein with HSV-1 and PML (light blue) for the respective samples in I cells. N = number of events counted. Means are indicated in the graphs in %.

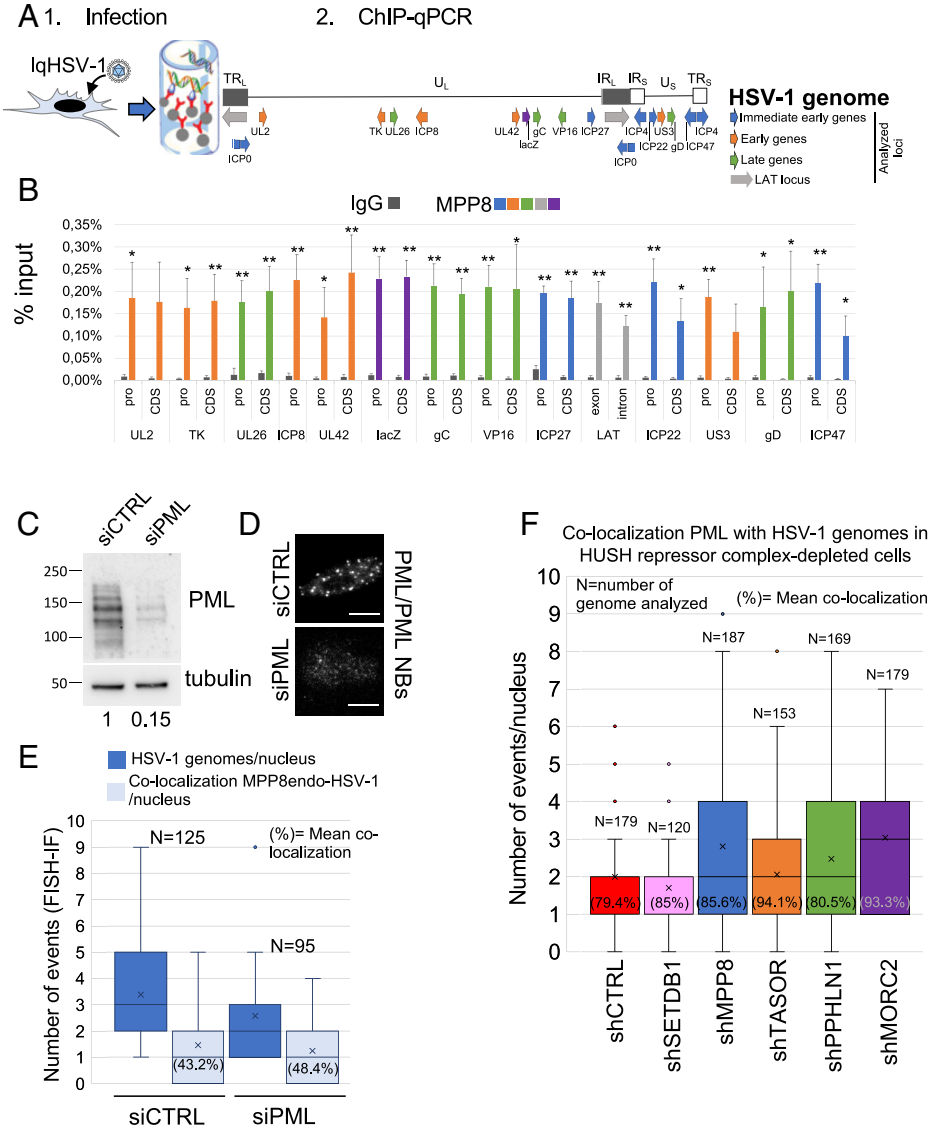

Fig. 2. Interaction of the proteins of the HUSH–SETDB1–MORC2 entity with the PML NB-associated quiescent HSV-1 genome. (*A*) Schematic view of the ChIP procedure to detect interactions of proteins with viral genomes. Control hFC or hFC expressing a tagged version of proteins of interest were infected with lqHSV-1 (m.o.i.= 3) and ChIP-qPCR was performed 24 h pi. All experiments were performed at least three times. Measurements were taken from distinct samples. Details about analyzed viral loci (names and sequences) are indicated in the *Materials and Methods* section. Quantification data are mean values (–SD). *P*-values * <0.05; ** <0.01 (one-tailed paired Student's *t* test). (*B*) Interaction of endogenous MPP8 with viral genome loci. Pro = promoter; CDS = coding sequence. (*C, D, E*) MPP8endo colocalization with lqHSV-1 in hFC transfected with a siRNA CTRL (siCTRL) or siRNA against PML (siPML) and infected with lqHSV-1 for 48 h (m.o.i. = 3). (*C*) WB of PML in siCTRL or siPML-treated hFC. The quantification of PML levels relative to tubulin (Tub) is depicted below the WB. (*D*) Representative images showing the PML signal by immunofluorescence (gray) to exemplify the efficiency of the siPML on PML NBs disappearance (also see ref. 31). (*E*) Quantification of the colocalization of MPP8endo with lqHSV-1 following immuno-FISH to detect MPP8, lqHSV-1, and PML. Distribution of HSV-1 genome signals/nucleus (dark blue) and colocalization of MPP8endo with lqHSV-1/nucleus (light blue) are shown. Means of colocalization between MPP8endo and lqHSV-1 are shown (in %). N = total number of viral genomes analyzed. (*F*) Quantification of PML colocalization with lqHSV-1 in hFC transduced with lentiviruses expressing control shRNA (shCTRL) or shRNA against proteins of interest and infected with lqHSV-1 for 48 h (m.o.i. = 3). Distribution of the numbers of colocalization between PML and lqHSV-1/nucleus are shown. Means of colocalization between PML and lqHSV-1 are shown (in %). N = total number of viral genomes analyzed.

and demonstrated its dependence on the activity of the HUSH–SETDB1–MORC2 repressor complex (Fig. 3 *H–I* and *SI Appendix*, Fig. S10*A*). As previously observed through ChIP-qPCR, depletion of TASOR led unexpectedly to a general increase in the H3K9me3 mark on the viral genome. Quantitative analysis of the viral reads associated with H3K9me3 across different conditions confirmed that, except for the shTASOR-treated cells, which showed a clear increase, the number of viral reads detected in infected cells treated with HUSH–SETDB1–MORC2 shRNAs was lower compared to control shRNA-treated cells (Fig. 3*J*). No viral reads were counted from uninfected cells (Fig. 3*J*). The overall reduction in the H3K9me3 mark on the lqHSV-1 genome did not stem from a general effect of the inactivation of the HUSH–SETDB1–MORC2 repressor complex, as this decrease was not universally observed across the cellular genome (Fig. 3*K*, chr21 gene-rich region as an example), and on previously identified H3K9me3-rich large heterochromatin regions (Fig. 3*L*, and *SI Appendix*, Fig. S10*B*) (32). As expected, peak annotation revealed that the majority of H3K9me3 peaks were linked with noncoding regions (distal intergenic and introns) (*SI Appendix*, Fig. S10 *C* and *D*). Conversely, no overall enrichment of the mark was detected on cellular enhancers and promoters (*SI Appendix*, Fig. S10*E*). Subsequently, our focus shifted toward families of long interspersed nuclear elements (LINEs) retrotransposons, which have been previously identified as undergoing significant regulation by components of the HUSH complex (21, 23, 24, 33, 34).

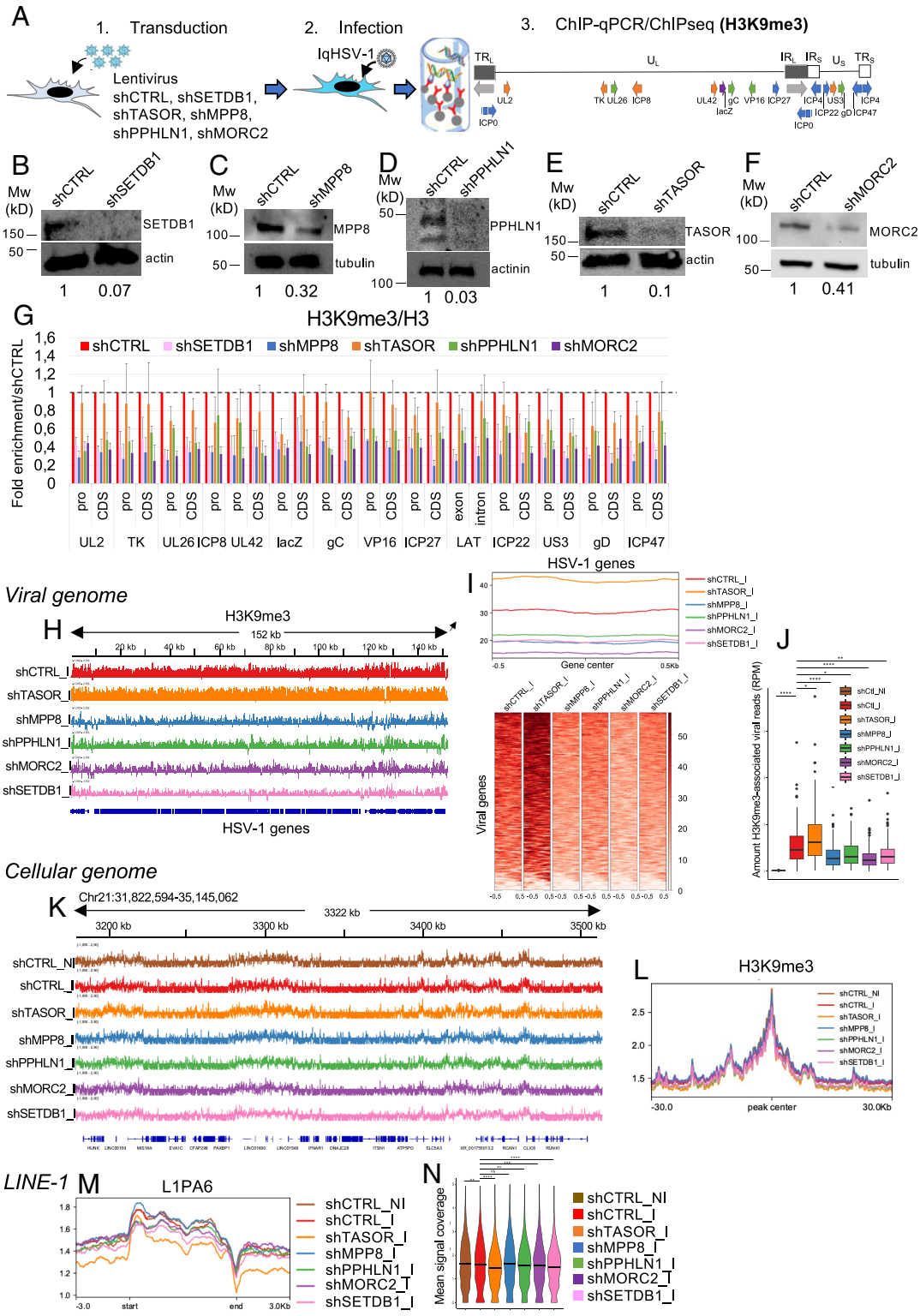

Fig. 3. Inactivation of proteins of the HUSH–SETDB1–MORC2 entity reduces H3K9me3 mark on the PML NB-associated quiescent HSV-1 genome. (*A*) Schematic view of the ChIP-qPCR/ChIP-seq procedure to detect enrichment of H3K9me3 on viral genomes after depletion or not by shRNAs of proteins of interest. Details about analyzed viral loci (names and sequences) are indicated in the Materials and Methods section. (*B–F*) WB on the target proteins to confirm the efficiency of the specific shRNAs. The quantification of protein levels relative to housekeeping proteins is depicted below the WBs. (*G*) ChIP-qPCR showing mean fold enrichments on the different viral loci of H3K9me3 in specific shRNA-depleted cells compared to cells expressing a control shRNA. Experiments were performed at least three times. H3K9me3 signal was standardized over total H3 present on each locus. Measurements were taken from distinct samples. Quantification data are mean values (±SD). For quantification details on each loci, see expanded *SI Appendix*, Fig. S6. *P*-values * <0.05; ** <0.01; *** <0.001 (one-tailed paired Student's *t* test). (*H–N*) Data from H3K9me3 ChIP-seq experiments in infected hFC treated with shCTRL or a shRNA against the indicated proteins of interest. (*H*) Genome browser snapshot of the H3K9me3 enrichment normalized on input across the entire quiescent HSV-1 genome. (*I*) Profile plot (*Top*) and heatmaps (*Bottom*) showing the density of H3K9me3 signal on HSV-1 genes. (*J*) Box plots showing the quantification of H3K9me3 reads on HSV-1 genes (in Reads Per Million). *P*-values * <0.05; ** <0.01; **** <0.0001 (nonparametric Wilcoxon rank-sum test). (*K*) Representative genome browser snapshot of the H3K9me3 enrichment normalized on input across a gene-rich region of chromosome 21. (*L*) Profile plot of the H3K9me3 density on large H3K9me3-rich regions defined in ref. 32. (*M*) Profile plots of the H3K9me3 density on a specific family of LINE-1 (L1PA6) regulated by HUSH. (*N*) ChIP-Seq mean signal coverage of H3K9me3 on L1PA6 across the different samples. The *Y* axis was adjusted to a 0 to 5 range. Adjusted *P*-values ** <0.01; *** <0.001; *** <0.001 (Wilcoxon rank-sum test), ns: nonsignificant.

As anticipated, the depletion of components within the HUSH–SETDB1–MORC2 complex, particularly TASOR, significantly affected the deposition of H3K9me3 on L1PA6 (Fig. 3 *M* and *N* for quantification of the signals; and *SI Appendix*, Fig. S10 *F* and *G* for additional families of LINEs).

These findings strengthen the role of HUSH core components, alongside SETDB1 and MORC2, as a key pathway in acquiring the repressive chromatin H3K9me3 mark on the PML NB-associated quiescent HSV-1 genome. Additionally, they suggest that TASOR inactivation may exert varying modulatory effects on H3K9me3 deposition depending on the integrated or episomal nature of specific genome loci.

The HUSH–SETDB1–MORC2 Entity Maintains PML NB-Associated HSV-1 Quiescence. LqHSV-1 is thermosensitive and acquires its quiescent state at 38.5 °C in hFC, leading to the formation of vDCP NBs and transcriptionally silent viral genomes. Latency can be reversed by destabilizing vDCP NBs with the HSV-1 protein ICP0 and reverting the temperature to 32 °C (7). To determine whether the HUSH complex is required to maintain lqHSV-1 silencing, individual components of the HUSH–SETDB1–MORC2 complex were depleted after the acquisition of the quiescent state and formation of the vDCP NBs (Fig. 4*A*). Inducible shRNA-mediated depletion (*SI Appendix*, Fig. S1 *A–E*) of HUSH complex components led to transcriptional activation of the lqHSV-1, as determined by the appearance of viral lytic gene-encoding mRNAs (Fig. 4 *B–E*). Additionally, within individual viral plaques visible in the cell monolayers displaying signs of reactivation (Fig. 4*F*), distinctive viral replication compartments (RC) indicative of ongoing viral lytic infections were easily identifiable. Notably, viral plaque formation was observed on hFC monolayers subsequent to HUSH depletion, contrasting the absence of plaque formation in the control (shCTRL) condition (*SI Appendix*, Fig. S11*F*). To confirm that inactivation of the HUSH complex induced production of infectious viral progeny, supernatants from the hFC monolayers were titrated on human bone osteosarcoma (U2OS) epithelial cells (Fig. 4 *G*, *up*). Supernatants from HUSH-depleted, but not shCTRL components induced viral plaque formation (Fig. 4*G*, supernatants of shCTRL and shMORC2 (shown as an example) and Fig. 4*H* for quantification). The HIV-2 and SIV Vpx accessory protein degrades TASOR and destabilizes the HUSH complex (35). Expression of HIV-2_{ROD} Vpx also induced transcriptional reactivation, appearance of RCs, and viral plaques (*SI Appendix*, Fig. S1 *A–D*) and production of infectious virus (*SI Appendix*, Fig. S12 *E* and *F*). However, presently, we cannot dismiss the possibility of additional effects of Vpx on the stability of other cellular targets, such as SAMHD1 (36, 37), or TASOR2 a paralog of TASOR recently described as being part of a HUSH2 complex (38, 39). These data demonstrate that the HUSH epigenetic repressor complex, along with SETDB1 and MORC2, is required for the stabilization of vDCP NBs and the PML NB-associated quiescence of HSV-1.

The Viral Protein ICP0 Induces the Proteasome-Dependent Degradation of MORC2. ICP0, a RING finger-containing E3 ubiquitin ligase, is recognized for its ability to trigger the proteasomal-dependent degradation of various cellular proteins, including PML, SP100, and MORC3 (40, 41). We examined the stability of HUSH–SETDB1–MORC2 proteins in cells infected with HSV-1WT or an ICP0-deficient virus (HSV-1ΔICP0 also known as dl1403) in the presence or absence of the proteasome inhibitor MG132. As anticipated, PML isoforms were degraded in an ICP0- and proteasome-dependent manner (Fig. 5*A*). The core proteins of the HUSH complex as well as SETDB1 remained unaffected in stability upon infection. Notably, MORC2 exhibited ICP0- and proteasome-dependent degradation (Fig. 5*B*). No significant effect on MORC2 mRNA abundance dependent on expression or not of ICP0 in infected cells could be detected (*SI Appendix*, Fig. S13). These data establish MORC2 as a potential critical regulator in maintaining HSV-1 quiescence in neurons.

MORC2 Maintains PML NB-Associated HSV-1 Quiescence in Human Neurons. The hFC infection model provides a practical system to characterize essential epigenetic features controlling PML NB-associated HSV-1 quiescence. As sensory neurons of the trigeminal ganglia (TG) are the predominant sites of latent HSV-1 infection including the formation of PML NB-associated quiescent HSV-1, it was essential to determine whether HUSH is also able to restrict HSV-1 infection in these cells. We therefore established PML NB-associated quiescent HSV-1 infection in human sensory neurons derived from human induced pluripotent stem cells (hiPSDN) (*SI Appendix*, Fig. S14*A*). These neurons recapitulate the molecular, electrophysiological, and biochemical features of sensory neurons in general, and nociceptive neurons in particular (*SI Appendix*, Fig. 14 *B–G*). HiPSDN exhibit PML NBs (*SI Appendix*, Fig. S14*H*), mirroring the presence observed in murine and human TG neurons (2, 3), and demonstrate the formation of vDCP NBs (*SI Appendix*, Fig. S14*I*). To confirm the validity of the hiPSDN infection model, we infected hiPSDN with the lqHSV-1 virus and measured reactivation following expression of the ICP0 viral protein or its inactive RING Finger domain mutant (ICP0RFmut) (Fig. 5*C*). ICP0, but not its RF mutant, destabilizes the PML NBs and vDCP NBs (7, 8) and induced transcriptional reactivation of lqHSV-1 (Fig. 5*D*), resulting in production of infectious viral progeny (Fig. 5 *E* and *F*). Immunofluorescent detection of the ICP4 and NF200 proteins further confirmed the presence of RCs in reactivating neurons (Fig. 5*G*). Finally, shRNA-mediated MORC2 depletion from lqHSV-1-infected hiPSDNs (Fig. 6*A* and *SI Appendix*, Fig. S15) also induced the transcriptional reactivation of lqHSV-1, as determined by the temporal increase in lytic viral mRNAs (Fig. 6*B*), confirming a role for the HUSH–MORC2 axis in the transcriptional silencing of PML NB-associated quiescent HSV-1. Furthermore, infectious progeny was released from reactivating neurons, as supernatants from day 7 shMORC2-treated neurons induced viral plaques in U2OS cells (Fig. 6 *C* and *D*). Taken together, these data demonstrate the essential role of MORC2, and by extension the HUSH complex, in maintaining PML-NB-associated HSV-1 quiescence in neurons.

Discussion

The neurotropic nature of HSV-1 and its ability to spread from the peripheral to the central nervous system makes it an important etiological candidate for nongenetic infection-associated neurodegenerative pathologies (43). It is therefore important to understand the mechanisms that induce and maintain HSV-1 in the latent state. The formation of repressive heterochromatin through K9me3 modification of histone H3.1 and/or histone variant H3.3 and chromatin compaction is an important mechanism for transcriptional silencing of endogenous retrotransposons and HIV as well as HSV-1 genomes, leading to the establishment of a latent/quiescent state (7, 12, 19, 21, 22, 44). Epigenetic regulation associated with viral chromatinization is therefore a hallmark of latent HSV-1. The HUSH–SETDB1–MORC2 repression complex is well described for its essential role in maintaining integrated retroelements in an inactive state (21, 27). MPP8 and SETDB1 interact and cooperate in the silencing of satellite DNA repeats in mouse

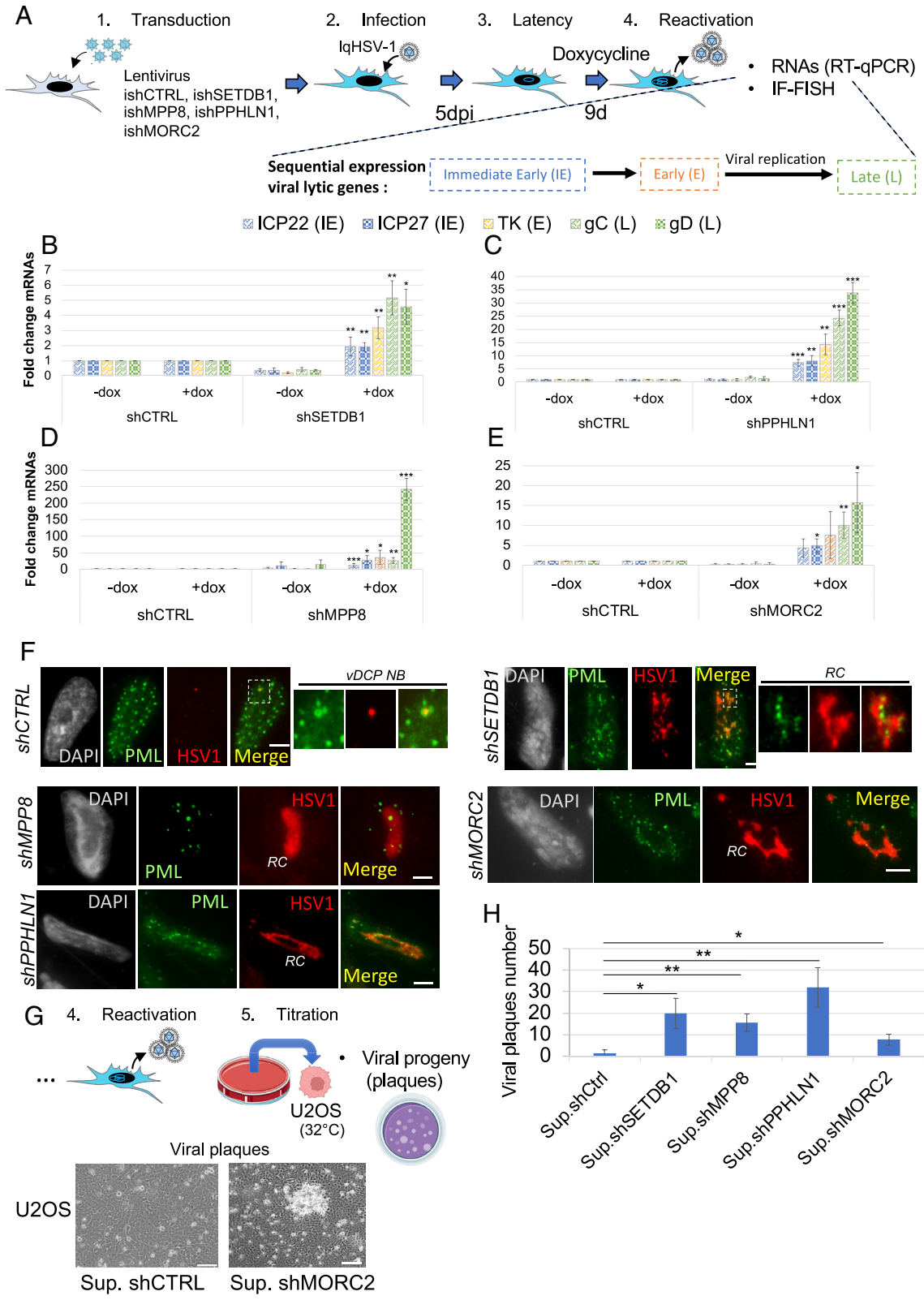

Fig. 4. The HUSH–SETDB1–MORC2 entity maintains the silencing of PML NB-associated quiescent HSV-1. (*A*) Schematic view of the experimental procedure to determine the restrictive activity of the individual proteins of the HUSH–SETDB1–MORC2 entity. hFC expressing inducible shRNA control (shCTRL) or shRNA against a protein of interest were infected with lqHSV-1 (m.o.i.= 3) at 38.5 °C to establish quiescence. 5 d later doxycycline was added for 9 d shifting the temperature at 32 °C to allow virus replication. Cells were used to perform RT-qPCR to quantify expression of viral lytic genes or immuno-FISH to detect viral RC. (*B–E*) RT-qPCR on representative HSV-1 lytic genes following treatment with a shCTRL, or a shRNA inactivating SETDB1, PPHLN1, MPP8, and MORC2, respectively. All experiments were performed at least three times. Measurements were taken from distinct samples. Quantification data are mean values (±SD). *P*-values * <0.05; ** <0.01; *** <0.001 (one-tailed paired Student's *t* test). (*F*) Immuno-FISH allowing the detection of PML (green), HSV-1 (red), and nuclei (gray, DAPI) in cell monolayers after induction of the shRNA CTRL, or targeting HUSH components (MPP8 and PPHLN1), or targeting SETDB1 or MORC2. (Scale bar, 5 μm.) RC: replication compartment. (*G*) Titration on U2OS cells of infectious viral progeny production from the above experiments using shRNA CTRL, or a shRNA inactivating each of the protein of the HUSH–SETDB1–MORC2 entity. *Up*: procedure; *Down*: viral plaques with supernatant from shMORC2 hFC shown as an example. (Scale bar, 100 μm.) (*H*) numerations of viral plaques from the above conditions.

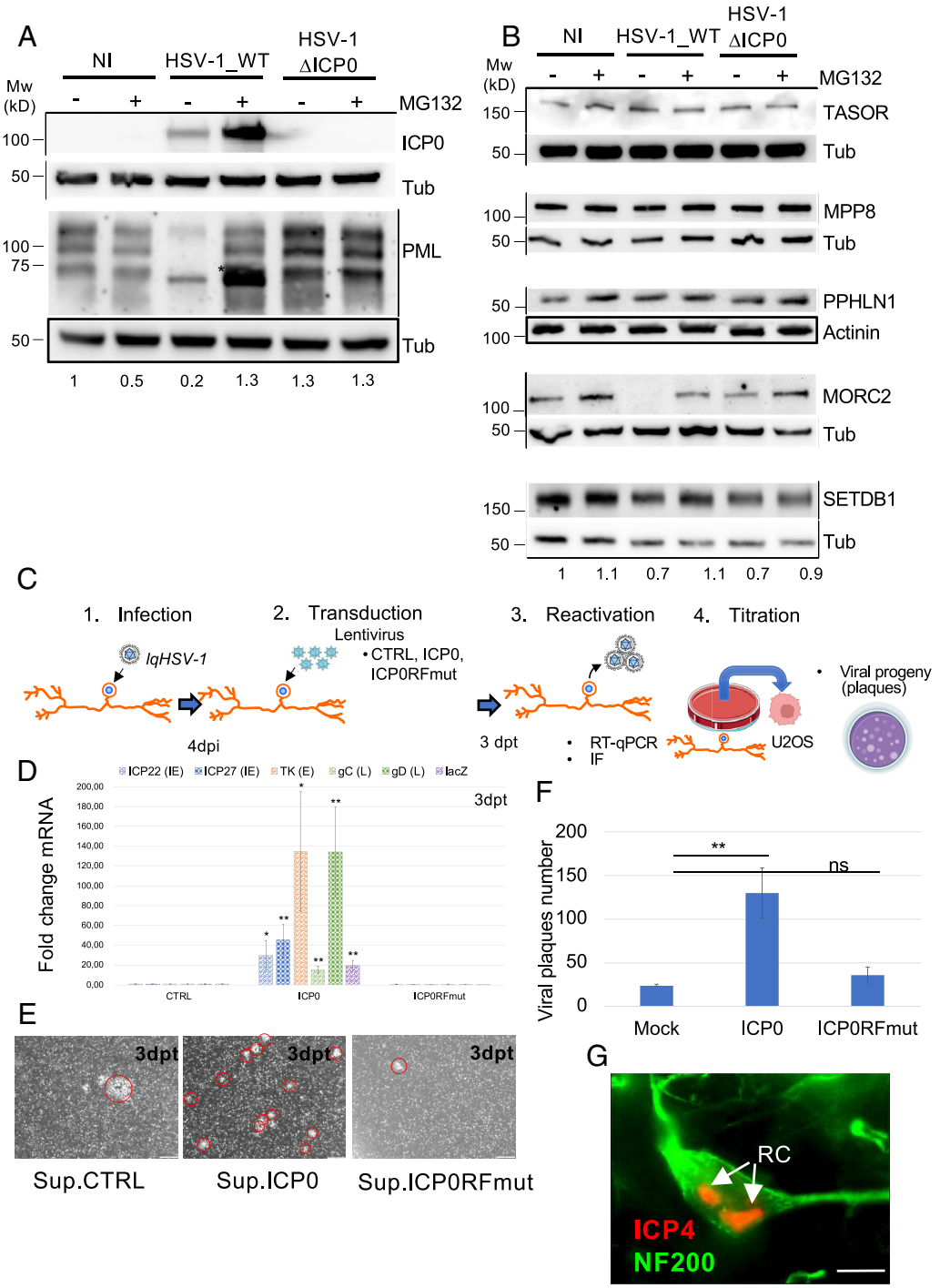

Fig. 5. ICP0 induces proteasomal-dependent degradation of MORC2 and reactivation of HSV-1 from quiescently infected neurons. (*A* and *B*) HFC were infected or not with wild-type HSV-1 (HSV) or a mutant HSV-1 unable to express ICP0 (HSVΔICP0), in the presence (+) or not (−) of the proteasome inhibitor MG132. (*A*) Detection of ICP0 expression and of PML. The star depicts the ICP0- and proteasome-dependent degradation of the SUMOylated forms of PML as first shown in ref. 42. (*B*) Detection of proteins of the HUSH complex, MORC2, and SETDB1. Tub or actinin were used as loading controls. Data are representative of at least two independent experiments that showed similar results. The quantification of protein levels relative to housekeeping proteins is depicted below the WBs. (*C*) Schematic view of the experimental procedure in hiPSDN infected with lqHSV-1 at 38.5 °C. 4 d after infection with lqHSV-1 neurons were transduced with lentiviruses control (CTRL) or expressing ICP0 or ICP0RFmut, and temperature was shifted to 32 °C to allow virus replication. Multiple analyses were performed at 3 d posttransduction (dpt). (*D*) RT-qPCR on representative HSV-1 lytic genes following expression of ICP0 (*Left*) or its nonfunctional mutant ICP0RFmut (*Right*). All experiments are in triplicates. All quantification data are mean values (±SD). Measurements were taken from distinct samples. *P*-values * <0.05; ** <0.01; *** <0.001 (one-tailed paired Student's *t* test). (*E*) Detection of viral plaques on U2OS cell monolayers in contact with supernatants from lqHSV-1 infected neurons transduced for 3 dpt with lentivirus CTRL or expressing ICP0 or ICP0RFmut. Crystal violet (grayscale) images for plaques (circled in red) visualization are shown. (Scale bar, 500 μm.) (*F*) Numeration of the plaques detected in (*E*). (*G*) Immunofluorescent detection of ICP4 (red) and NF200 (green) showing viral RC in neurons. Arrows point out two RCs in the same nucleus of a single neuron. (Scale bar, 10 μm.)

embryonic stem cells (45). The HUSH complex, together with NP220/ZNF638, also silences nonintegrated MLV (26). Similarly, NP220 and HUSH silence recombinant AAV (rAAV) vectors in a serotype-dependent manner (25). However, the actual contribution of HUSH in maintaining latency of a genuine unintegrated episomal virus such as HSV-1 has not been determined.

We and others have demonstrated the heterogeneity of HSV-1 latency in neurons in vivo in mouse models. This heterogeneity exists

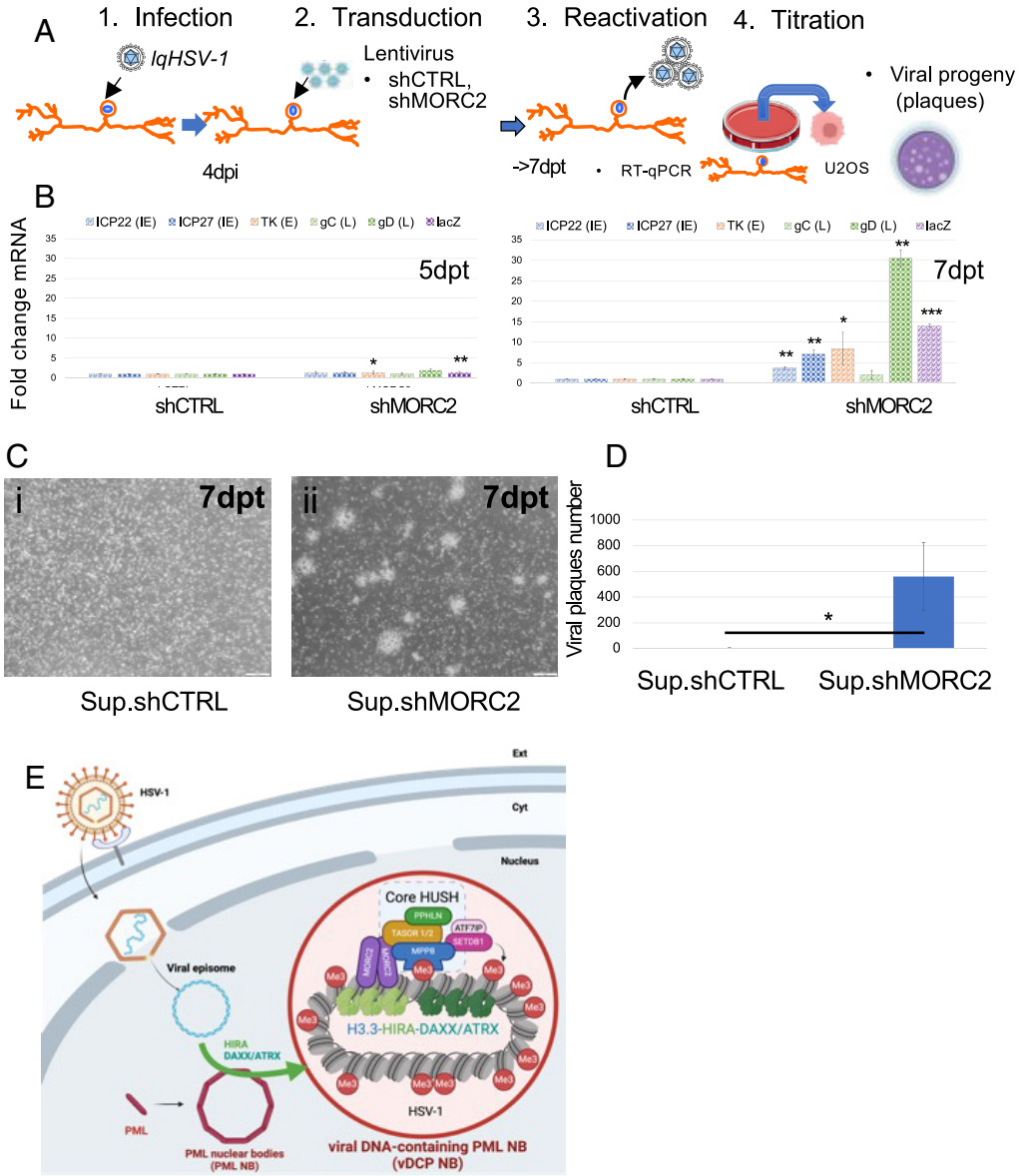

Fig. 6. The HUSH–SETDB1–MORC2 entity acts as a restriction pathway in neurons infected with HSV-1. (*A*) Schematic view of the experimental procedure to determine the restriction activity of the HUSH–SETDB1–MORC2 entity in hiPSDN infected with lqHSV-1 at 38.5 °C. 4 d after infection with lqHSV-1 neurons were transduced with lentiviruses expressing a shRNA control, or a shRNA against MORC2, and temperature was shifted to 32 °C to allow virus replication. Multiple analyses were performed 5 and 7 d posttransduction (dpt). (*B*) RT-qPCR at 5dpt (*Left*) and 7dpt (*Right*) on representative HSV-1 lytic genes following treatment with a shRNA CTRL (shCTRL), or a shRNA inactivating MORC2. All experiments are in triplicates. Measurements were taken from distinct samples. All quantification data are mean values (±SD). *P*-values * <0.05; ** <0.01 (one-tailed paired Student's *t* test). (*C*) Detection of viral plaques in U2OS cells monolayers in contact with supernatants from shCTRL i) or shMORC2 ii) treated lqHSV-1 infected neurons. Crystal violet (grayscale) images for plaque visualization are shown. (Scale bar, 100 μm.) (*D*) Numeration of viral plaques from *C*. *P*-values * <0.05 (one-tailed paired Student's *t* test). Measurements were taken from distinct samples. Crystal violet images (grayscale) of U2OS cell monolayers are shown above each condition. (Scale bar, 500 μm.) (*E*) Model of epigenetic restriction of nuclear incoming HSV-1 DNA by the HUSH–SETDB1–MORC2 entity through the apposition of trimethyl marks on H3K9 on the chromatinized viral genome ultimately leading to PML NB-associated quiescent HSV-1 genomes. Made with BioRender.

at least at the level of viral genome chromatin marks acquisition and interaction of latent viral genomes with the nuclear environment (2, 12, 13, 46). The latter is exemplified by the encapsulation of the viral genomes in a quiescent state within PML NBs and referred as to vDCP NBs (2, 3). In the present study, we decipher a mechanism of establishment and maintenance of PML NB-associated quiescent HSV-1 genomes involving the apposition of the H3K9me3 mark on the viral chromatin by the HUSH–SETDB1–MORC2 repression complex. We show that his pathway is closely associated with, but independent of the formation of vDCP NBs. The HUSH–SETDB1–MORC2 complex is essential for the acquisition of the H3K9me3 chromatin mark on quiescent HSV-1 genomes, in a viral genome sequence–independent manner, and for their transcriptional repression. The interaction of SETDB1 with the H3.3-chromatinized viral genome to induce trimethylation of H3K9 could serve as a mechanism to recruit the HUSH–MORC2 complex across the entire viral genome, via the interaction between SETDB1 and MPP8, as demonstrated in mouse embryonic stem cells (47). Questions may arise regarding the apparent absence of a role of TASOR at least in relation to the deposition of the H3K9me3 mark on quiescent HSV-1. These observations may need to be reconsidered in light of recent findings regarding the existence of a HUSH2 complex containing TASOR2, a paralog of TASOR, that may impact the activity of HUSH (38, 39). A functional HUSH–SETDB1–MORC2 complex is also essential for maintaining PML NB-associated HSV-1 quiescence in neuronal cells, as suggested by

the importance of MORC2 in the control of the stability of HSV-1 quiescence in hiPSDN. Given the essential role of MORC2 for the HUSH complex activity (27), this suggests that the HUSH–SETDB1–MORC2 repression complex acts as a major epigenetic regulatory entity to maintain PML NB-associated HSV-1 quiescence in neurons.

Accordingly, we found that MORC2 is a specific target of the viral protein ICP0 for degradation mediated by the proteasome. We and others have already published that ICP0 has multiple cellular targets to prevent the antiviral response [for reviews (48)]. Our results suggest that instead of targeting one of the three components of the HUSH complex for degradation, which would allow MORC2 to function independently, ICP0 specifically induces the degradation of MORC2. This, in turn, disrupts the entire SETDB1-HUSH–MORC2 repressor complex. It is already known that ICP0 impacts the stability of MORC3, a gatekeeper of the antiviral response (41, 49). The additional degradation of MORC2 mediated by ICP0 is thus of most importance and suggests that the virus has evolved to counteract the activity of the proteins of the entire MORC family, which comprises four members. This anticipates that proteins of the MORC family are major restriction factors that evolved to counteract HSV infection. Another important aspect regarding MORC2 is that it has been described together with MPP8 as a major component of neurons playing a major role in neuron homeostasis by repressing the protocadherin gene cluster, which play crucial roles in the development and function of the nervous system, particularly in neuronal connectivity and synaptic specificity (50). It is thus very interesting to see that a neurotropic virus such as HSV-1, which establishes latency in sensory neurons, has evolved as such as its viral protein essential for full reactivation, ICP0, targets MORC2 for degradation. SETDB1 is also known for its major involvement in neuron survival and brain development (51). The involvement of the HUSH–SETDB1–MORC2 entity in the acute control, then long-term maintenance, of one of the latency-associated molecular patterns of a neurotropic virus is thus of particular interest.

The association of the HUSH–SETDB1–MORC2 entity with vDCP NBs most likely links its epigenetic activity with the stability of the vDCP NBs. The HSV-1 ICP0 protein destabilizes PML NBs and vDCP NBs (7) and has been shown to erase the H3K9me3 mark on viral chromatin upon HSV-1 lytic cycle and establishment/maintenance of latency (52). We show that ICP0 is able to induce HSV-1 reactivation in quiescently infected iPSDN. This suggests that ICP0 directly and indirectly affects the activity of the HUSH–SETDB1–MORC2 entity by destabilizing both the vDCP NBs and the HUSH repressor complex.

The HUSH–SETDB1–MORC2 entity acting as a nuclear restriction pathway in concert with the activity of PML NBs, extends at the epigenetic level the intrinsic response of the cell for the control of the infection by a neurotropic virus (Fig. 6*E*). This pathway is a direct target of the activity of the viral protein ICP0, likely through the proteasomal degradation of MORC2 in addition to the destabilization of vDCP NBs, to promote reactivation of HSV-1. Stabilizing this important pathway would enable the control of neuronal damage caused by the spread of the virus in the nervous system following reactivation. Alternatively, destabilizing the HUSH–SETDB1–MORC2 entity might be considered a complementary approach to proposed therapies designed to modify viral genomes to prevent their reactivation. As an example, viral genome editing using meganucleases or CRISPR/Cas9 technologies has been proposed to eliminate latent HSV reservoirs (53, 54). Provoking subreactivation of HSV-1 by inactivating the HUSH–SETDB1–MORC2 entity could then potentiate the use of these technologies, provided that it does not induce global epigenetic modifications that would put a threat on cellular defense mechanisms. On a different aspect, targeting HUSH for degradation has been discussed as part of a "shock and kill" strategy in HIV cure designed to eliminate reservoir cells responsible for rebounds when antiretroviral treatments are stopped (55). Our study establishes HUSH as a crucial factor in maintaining PML NB-associated HSV-1 quiescence. Targeting HUSH degradation, moreover in immunocompromised patients, without controlling herpesvirus lytic cycle, e.g., by administration of anti-herpesviral drugs, could therefore compromise the integrity of patients. Indeed, this could lead to uncontrolled HSV-1 spread in the PNS and CNS potentially responsible for neuronal and/or ocular pathologies as a result of herpesvirus reactivation. In that context, the "block and lock" strategy to create a "deep latency" of HIV seems indeed more appropriate considering the likely broad involvement of the HUSH–SETDB1–MORC2 entity in the control of multiple latent viruses. Finally, the importance of the HUSH–SETDB1–MORC2 repression complex together with PML NBs to control a genuine unintegrated virus, such as HSV-1, could be broadened to other viruses remaining latent/quiescent as episomes in the nucleus of infected cells.

Materials and Methods

Virus Strains and Cells. Viruses used for the study (7) and human induced pluripotent stem (hiPS) (56) were previously described. See *SI Appendix, Supplementary Materials and Methods* for details on viruses and cells and for protocols on cell growth.

Generation of Sensory Neurons with Nociceptive Properties and Electrophysiology. Differentiation of hiPSC into sensory neurons was performed according to ref. 57. Detailed protocols for hiPSC growth, differentiation into sensory neurons with nociceptive properties, and electrophysiology measurements are provided in *SI Appendix, Supplementary Materials and Methods*.

Lentivirus Production and Establishment of Cell Lines. Plasmids of interest were cotransfected with psPAX.2 (Addgene #12260) and pMD2.G (Addgene #12259) plasmids with a ratio of 3:2:1 by the calcium phosphate method into HEK 293 T cells to package lentiviral particles. hFC or hiPSDN cells stably expressing transgenes or shRNA were obtained by lentiviral transduction. See *SI Appendix, Supplementary Materials and Methods* for detailed protocol.

Immunofluorescence, DNA FISH, and Immune-FISH. For immunofluorescence, cells were treated according to ref. 7. HSV-1 DNA FISH probes consisting of cosmids 14, 28, and 56 (7) comprising a total of ~90 kb of the HSV-1 genome were labeled by nick-translation (Invitrogen) with dCTP-Cy3 (GE Healthcare) and stored in 100% formamide (Sigma). The DNA-FISH and immuno-DNA FISH procedures have been described previously (2). See *SI Appendix, Supplementary Materials and Methods* for detailed protocol.

Microscopy, Imaging, and Quantification. Images were acquired with the Axio Observer Z1 inverted wide-field epifluorescence microscope (100× or 63× objectives/N.A. 1.46 or 1.4) (Zeiss) and a CoolSnap HQ2 camera from Photometrics. Identical settings and contrast were applied for all images of the same experiment to allow data comparison through ImageJ.

ChIP-quantitative PCR and ChIP Sequencing. For ChIP-quantitative PCR, see *SI Appendix, Supplementary Materials and Methods* for detailed protocol. For ChIP-sequencing, hFC were transduced with fresh lentiviruses encoding shRNAs against the HUSH complex, MORC2, or SETDB1 (see section "plasmids" in *SI Appendix, Supplementary Materials and Methods*) for 48 h to allow the depletion of the specific proteins, before being infected with HSV-1 *in1374* at an m.o.i. of 3 for 24 h. Cells were then cross-linked and processed for ChIP as described previously (31). Twenty μL of protein A magnetic dynabeads (Invitrogen, 10001D) were used for immunoprecipitation with 2 μg of the H3K9me3 antibody (see *SI Appendix, Supplementary Materials and Methods* for antibody details). After ChIP, libraries were prepared with 10 ng of DNA (input/ChIP) using the NEBNext® UltraTM II DNA Library Prep Kit for Illumina. DNA libraries were then sequenced using the paired-end method (2 × 150pb) on the Element Biosciences Aviti (HELIXIO,

Clermont-Ferrand, France). Raw reads were filtered by trimming Illumina adapters and removing low-quality reads using Trimmomatic (v.0.39) with default parameters. Trimmed reads (containing more than 36 nucleotides) were aligned to the human (hg38) reference genome concatenated with the HSV-1 genome (GCF_000859985.2.fa) using bowtie2 (v2.5.1). For detailed analyses of ChIP-seq data, see *SI Appendix, Supplementary Materials and Methods*.

siRNA Transfections. Transfections of hFC with siRNAs were performed using Lipofectamine RNAiMAX and following the supplier's procedure (Thermo Fisher Scientific). The following siRNAs were used at a final concentration of 40 nM for 48 h: siCTRL (siluc): 5′-CGUACGCGGAAUACUUCGA, siSETDB1: 5′-ACCCGAGGCUUUGCUCUUA, and siPML: 5′-AGATGCAGCTGTATCCAAG.

Reactivation Procedures.

hFC. Cells were transduced with pLKO-tet-On-shRNA to produce hFC-ishRNA stably and inducibly expressing the ishRNA (selection puro 1μg/mL). FBS Tetracycline free (CliniSciences, FBS-TET-12A) was used to prevent ishRNA expression. hFC-ishRNA were infected with lqHSV-1 for 4 d at 38.5 °C to stabilize the formation of vDCP NBs. Then, the expression of shRNA was induced by the addition of doxycycline (1μg/mL) in the medium. Cells were incubated at 32 °C the permissive temperature for lqHSV-1 (see section "Virus strains and cells" in *SI Appendix, Supplementary Materials and Methods*). From day 8 to day 10 after addition of doxycycline, the cells were fixed to proceed to immuno-FISH analyses, or RNA was extracted to perform RT-qPCR (*RT-qPCR*).

HiPSDN. HiPSDN were cultured for at least 24 h without antimitotic agents prior to infection with lqHSV-1. HiPSDN were infected with the indicated virus at 3.10e5 PFU/wells for 1h30 at 37 °C. Postinfection, inoculum was replaced with neurobasal containing NGF (20 ng/mL) and NT3 (10 ng/mL). After 4 d at 38 °C, neurons were transduced with the indicated lentivirus (see section "Lentivirus production and establishment of cell lines" in *SI Appendix, Supplementary Materials and Methods*). The next day, transduced neurons were put at 32 °C (the permissive temperature for replication) during the indicated times. Human Serum (1%) was added to the media to limit cell-to-cell spread. Reactivation was quantified by RT-qPCR of HSV-1 lytic mRNAs isolated from the cells in culture. The same experiment was performed but without Human serum to recover the supernatant. Reactivation was quantified by the production of infectious viral particles through supernatant titration.

RT-qPCR. RNAs were extracted according to The Qiagen RNeasy Mini Kit manufactured protocol (Qiagen, Valencia, CA). RNAs were treated 30 mn at 37 °C with DNAseI (Thermo Fisher). Then, 1μg was taken to perform RT with RevertAID Reverse Transcriptase (Thermo Fisher). cDNA was then resuspended in water and kept at −20 °C until use for qPCR. Quantitative PCRs were performed using the KAPA SYBR qPCR Master Mix (SYBR Green I dye chemistry) (KAPA BIOSYSTEMS, KK4618) and the CFX connect apparatus (Bio-Rad). Primers used are described here below. See *SI Appendix, Supplementary Materials and Methods* for primers.

Western blotting. RIPA extracts were obtained by lysing the cells in RIPA buffer (50 mM Tris-HCl pH 7.5, 150 mM NaCl, 0,5% Na-Deoxycholate, 1% NP-40, 0,1% SDS, and 5 mM EDTA) supplemented with 1× protease inhibitor cocktail for 20 min on ice. See *SI Appendix, Supplementary Materials and Methods* for detailed protocol.

Antibodies. See *SI Appendix, Supplementary Materials and Methods* for antibodies used.

Data, Materials, and Software Availability. The ChIP-Seq datasets have been deposited in the Gene Expression Omnibus (GEO; http://www.ncbi.nlm.nih.gov/geo/query/acc.cgi?) under Accession No. GSE263436 (58). All other data are included in the manuscript and/or *SI Appendix*.

ACKNOWLEDGMENTS. We thank Prof. Roger Everett (Center for Virus Research, University of Glasgow, UK) for the *in*1374/lqHSV-1 virus and ICP0-expressing lentivirus vectors, Dr. Slimane Ait-Si-Ali (Epigenetic and cell fate, University Paris Diderot, France) for SETDB1 constructs, Prof. Delphine Poncet (INMG-PGNM) for advices on statistical analyses, and Dr. Thomas Simonet (INMG-PGNM) for precious advice on bioinformatic analyses. The INMG-PGNM laboratory is funded by grants from the Centre National de la Recherche Scientifique (CNRS), Institut National de la Santé et de la Recherche Médicale (Inserm), University Claude Bernard Lyon 1, and AFM-téléthon. This work was financially supported by the French National Agency for Research-ANR through grants ANR-18-CE15-0014-01, ANR-20-COV9-0004-01, ANR-21-CE17-0018, LabEX DEV2CAN (ANR-10-LABX-61), ligue contre le cancer, and ANRS (ECTZ188412, ECTZ159208), AFM-téléthon (MyoNeuRALP2). P.L. team is member of the Groupements de Recherche, Dynamique des interactions entre chromatines virale et cellulaire (DYNAVIR, GDR2194), and Architecture et Dynamique du Noyau & des Génomes (ADN&G) funded by the CNRS. P.J.L. is supported by a Wellcome Trust Principal Research Fellowship ((210688/Z/18/Z), Wellcome Trust Discovery Award (227418/Z/23/Z) and MRC Project grant (MR/V011561/1). P.L. is a CNRS Research Director.

Author affiliations: [a]Université Claude Bernard Lyon 1, Centre national de la recherche scientifique (CNRS) UMR 5261, Institut national de la santé et de la recherche médicale (Inserm) U1315, Laboratoire d'Excellence (LabEx) DEV2CAN, Institut NeuroMyoGène-Pathophysiology and Genetics of Neuron and Muscle (INMG-PGNM), team "Chromatin dynamics, Nuclear Domains, Virus", Lyon 69008, France; [b]SupBiotech Research Department - CellTechs Laboratory, SupBiotech, Lyon 69003, France; [c]Institut Universitaire de France (IUF), Paris 75005, France; [d]Faculty of Medicine Department of Cellular and Molecular Medicine University of Ottawa, Ottawa, ON K1H 8M5, Canada; [e]Cambridge Institute of Therapeutic Immunology and Infectious Disease, Jeffrey Cheah Biomedical Centre, Cambridge CB2 OAW, United Kingdom; [f]Université Montpellier, Centre national de la recherche scientifique (CNRS) UMR5294, Laboratory of Pathogen Host Interactions (LPHI), team "GATAC-Malaria", Montpellier 34095, France; [g]Université Paris-Saclay, Institut national de la santé et de la recherche médicale (Inserm), U1184, Center for Immunology of Viral, Auto-immune, Hematological and Bacterial diseases (IMVA-HB). Commissariat à l'Énergie Atomique et aux Énergies renouvelables (CEA), Fontenay-aux-Roses 92260, France; [h]Université Claude Bernard Lyon 1, Centre national de la recherche scientifique (CNRS) UMR 5284, Institut national de la santé et de la recherche médicale (Inserm) U1314, Institut NeuroMyoGène-Mechanisms in Integrated Life Sciences (INMG-MeLiS), Team "Synaptopathies et Autoanticorps", Lyon 69008, France; [i]Université Paris Cité, Institut Cochin, Centre national de la recherche scientifique (CNRS) UMR 8104, Institut national de la santé et de la recherche médicale (Inserm) U1016, Paris 75014, France; [j]Université Aix-Marseille, Institut national de la santé et de la recherche médicale (Inserm) U1251, Marseille Medical Genetics (MMG), team "Epigenetic and nucleoskeleton dynamics in rare diseases", Marseille 13385, France; [k]Université Paris-Saclay, Service d'Ophtalmologie, Hôpital Bicêtre, Assistance Publique - Hôpitaux de Paris (AP-HP), Centre de Recherche Maladies Rares (CMR), Centre de référence des maladies rares en ophtalmologie (OPHTARA), Le Kremlin-Bicêtre 94270, France; and [l]Service d'Ophtalmologie, Hôpital National de la Vision des Quinze-Vingts, Institut Hospitalo-universitaire (IHU) FOReSIGHT, Paris 75012, France

Author contributions: S.R., T.E., F.J., A.C., P.J.L., and P.L. conceived the study; S.R., T.E., F.J., A.C., M.L., F.M., P.J.L., and P.L. designed experiments and interpreted data; S.R., T.E., F.J., A.C., R.N., O.B., C.S., M.G., C.C., P.T., O.H., O.P., Y.G., and M.L. performed experiments; F.M. developed the hiPSC and contributed to the hiPSDN differentiation protocol; A.C. and S.B. contributed to the development and production of lentiviruses; O.P. performed the electrophysiological experiments for hiPSDN; S.R., T.E., F.J., A.C., R.N., O.B., C.S., M.G., S.B., C.C., P.T., O.H., O.P., Y.G., F.M., M.L., P.J.L., and P.L. reviewed and edited the manuscript; and S.R., T.E., F.J., A.C., P.J.L., and P.L. wrote the paper.

1. D. M. Knipe, A. Cliffe, Chromatin control of herpes simplex virus lytic and latent infection. *Nat. Rev. Microbiol.* **6**, 211–221 (2008).
2. F. Catez *et al.*, HSV-1 genome subnuclear positioning and associations with host-cell PML-NBs and centromeres regulate LAT locus transcription during latency in neurons. *PLoS Pathog.* **8**, e1002852 (2012).
3. M.-A. Maroui *et al.*, Latency entry of herpes simplex virus 1 Is determined by the interaction of its genome with the nuclear environment. *PLoS Pathog.* **12**, e1005834 (2016).
4. A. Corpet *et al.*, PML nuclear bodies and chromatin dynamics: Catch me if you can! *Nucleic Acids Res.* **389**, 251 (2020).
5. R. D. Everett, J. Murray, A. Orr, C. M. Preston, Herpes simplex virus type 1 genomes are associated with ND10 nuclear substructures in quiescently infected human fibroblasts. *J. Virol.* **81**, 10991–11004 (2007).
6. T. Alandijany *et al.*, Distinct temporal roles for the promyelocytic leukaemia (PML) protein in the sequential regulation of intracellular host immunity to HSV-1 infection. *PLoS Pathog.* **14**, e1006769 (2018).
7. C. Cohen *et al.*, Promyelocytic leukemia (PML) nuclear bodies (NBs) induce latent/quiescent HSV-1 genomes chromatinization through a PML NB/Histone H3.3/H3.3 Chaperone Axis. *PLoS Pathog.* **14**, e1007313 (2018).
8. R. D. Everett *et al.*, A novel ubiquitin-specific protease is dynamically associated with the PML nuclear domain and binds to a herpesvirus regulatory protein. *Embo J.* **16**, 1519–1530 (1997).
9. W. P. Halford, P. A. Schaffer, ICP0 is required for efficient reactivation of herpes simplex virus type 1 from neuronal latency. *J. Virol.* **75**, 3240–3249 (2001).
10. R. L. Thompson, N. M. Sawtell, Evidence that the herpes simplex virus type 1 ICP0 protein does not initiate reactivation from latency in vivo. *J. Virol.* **80**, 10919–10930 (2006).
11. C. Boutell *et al.*, A viral ubiquitin ligase has substrate preferential SUMO targeted ubiquitin ligase activity that counteracts intrinsic antiviral defence. *PLoS Pathog.* **7**, e1002245 (2011).
12. Q.-Y. Wang *et al.*, Herpesviral latency-associated transcript gene promotes assembly of heterochromatin on viral lytic-gene promoters in latent infection. *Proc. Natl. Acad. Sci. U.S.A.* **102**, 16055–16059 (2005).
13. A. R. Cliffe, D. M. Coen, D. M. Knipe, Kinetics of facultative heterochromatin and polycomb group protein association with the herpes simplex viral genome during establishment of latent infection. *mBio* **4**, e00590 (2013).
14. A. K. Francois *et al.*, Single-genome analysis reveals a heterogeneous association of the herpes simplex virus genome with H3K27me2 and the reader PHF20L1 following infection of human fibroblasts. *mBio* **15**, e0327823 (2024), 10.1128/mbio.03278-23.

15. Y. Liang, J. L. Vogel, A. Narayanan, H. Peng, T. M. Kristie, Inhibition of the histone demethylase LSD1 blocks alpha-herpesvirus lytic replication and reactivation from latency. *Nat. Med.* **15**, 1312–1317 (2009).
16. T. M. Kristie, Chromatin modulation of herpesvirus lytic gene expression: Managing nucleosome density and heterochromatic histone modifications. *mBio* **7**, e00098 (2016).
17. L. Yang *et al.*, Molecular cloning of ESET, a novel histone H3-specific methyltransferase that interacts with ERG transcription factor. *Oncogene* **21**, 148–152 (2002).
18. S. Cho, J. S. Park, Y.-K. Kang, Dual functions of histone-lysine N-methyltransferase Setdb1 protein at promyelocytic leukemia-nuclear body (PML-NB): Maintaining PML-NB structure and regulating the expression of its associated genes. *J. Biol. Chem.* **286**, 41115–41124 (2011).
19. T. Matsui *et al.*, Proviral silencing in embryonic stem cells requires the histone methyltransferase ESET. *Nature* **464**, 927–931 (2010).
20. B. Rauwel *et al.*, Release of human cytomegalovirus from latency by a KAP1/TRIM28 phosphorylation switch. *eLife* **4**, 1208 (2015).
21. I. A. Tchasovnikarova *et al.*, Epigenetic silencing by the HUSH complex mediates position-effect variegation in human cells. *Science* **348**, 1481–1485 (2015).
22. M. Seczynska, S. Bloor, S. M. Cuesta, P. J. Lehner, Genome surveillance by HUSH-mediated silencing of intronless mobile elements. *Nature* **601**, 1–9 (2021), 10.1038/s41586-021-04228-1.
23. L. Robbez-Masson *et al.*, The HUSH complex cooperates with TRIM28 to repress young retrotransposons and new genes. *Genome Res.* **28**, 836–845 (2018).
24. N. Liu *et al.*, Selective silencing of euchromatic L1s revealed by genome-wide screens for L1 regulators. *Nature* **553**, 228–232 (2018).
25. A. Das *et al.*, Epigenetic silencing of recombinant adeno-associated virus genomes by NP220 and the HUSH complex. *J. Virol.* **96**, e0203921 (2022).
26. Y. Zhu, G. Z. Wang, O. Cingöz, S. P. Goff, NP220 mediates silencing of unintegrated retroviral DNA. *Nature* **564**, 278–282 (2018).
27. I. A. Tchasovnikarova *et al.*, Hyperactivation of HUSH complex function by Charcot-Marie-Tooth disease mutation in MORC2. *Nat. Genet.* **49**, 1035–1044 (2017).
28. O. M. Albulym *et al.*, MORC2 mutations cause axonal Charcot–Marie–Tooth disease with pyramidal signs. *Ann. Neurol.* **79**, 419–427 (2016).
29. D. Ray-Gallet *et al.*, Dynamics of histone h3 deposition in vivo reveal a nucleosome gap-filling mechanism for h3.3 to maintain chromatin integrity. *Mol. Cell* **44**, 928–941 (2011).
30. G. Banumathy *et al.*, Human UBN1 Is an ortholog of yeast Hpc2p and has an essential role in the HIRA/ASF1a chromatin-remodeling pathway in senescent cells. *Mol. Cell Biol.* **29**, 758-770 (2009).
31. C. Kleijwegt *et al.*, Interplay between PML NBs and HIRA for H3.3 dynamics following type I interferon stimulus. *eLife* **12**, e80156 (2023).
32. J. S. Becker *et al.*, Genomic and proteomic resolution of heterochromatin and its restriction of alternate fate genes. *Mol. Cell* **68**, 1023–1037.e15 (2017).
33. H. Tunbak *et al.*, The HUSH complex is a gatekeeper of type I interferon through epigenetic regulation of LINE-1s. *Nat. Commun.* **11**, 5387 (2020).
34. Z. Li *et al.*, Asymmetric distribution of parental H3K9me3 in S phase silences L1 elements. *Nature* **623**, 643-651 (2023), 10.1038/s41586-023-06711-3.
35. G. Chougui *et al.*, HIV-2/SIV viral protein X counteracts HUSH repressor complex. *Nat. Microbiol.* **3**, 891–897 (2018).
36. N. Laguette *et al.*, SAMHD1 is the dendritic- and myeloid-cell-specific HIV-1 restriction factor counteracted by Vpx. *Nature* **474**, 654–657 (2011).
37. K. Hrecka *et al.*, Vpx relieves inhibition of HIV-1 infection of macrophages mediated by the SAMHD1 protein. *Nature* **474**, 658–661 (2011).
38. Z. D. Jensvold, J. R. Flood, A. E. Christenson, P. W. Lewis, Interplay between two paralogous human silencing hub (HuSH) complexes in regulating LINE-1 element silencing. *Nat. Commun.* **15**, 9492 (2024).
39. J. M. C. Danac *et al.*, Competition between two HUSH complexes orchestrates the immune response to retroelement invasion. *Mol. Cell* **84**, 2801–2803 (2024), 10.1016/j.molcel.2024.06.020.
40. M. K. Chelbi-Alix, H. de The, Herpes virus induced proteasome-dependent degradation of the nuclear bodies-associated PML and Sp100 proteins. *Oncogene* **18**, 935–941 (1999).
41. E. Sloan, A. Orr, R. D. Everett, MORC3, a component of PML Nuclear Bodies, has a role in restricting herpes simplex virus type 1 and human cytomegalovirus. *J. Virol.* **90**, 8621–8633 (2016), 10.1128/jvi.00621-16.
42. R. Everett *et al.*, The disruption of ND10 during herpes simplex virus infection correlates with the Vmw110- and proteasome-dependent loss of several PML isoforms. *J. Virol.* **72**, 6581-6591 (1998).
43. M. E. Marcocci *et al.*, Herpes simplex virus-1 in the brain: The dark side of a sneaky infection. *Trends Microbiol.* **28**, 808-820 (2020), 10.1016/j.tim.2020.03.003.
44. S. J. Elsässer, K.-M. Noh, N. Diaz, C. D. Allis, L. A. Banaszynski, Histone H3.3 is required for endogenous retroviral element silencing in embryonic stem cells. *Nature* **522**, 240–244 (2015).
45. P. Cruz-Tapias, P. Robin, J. Pontis, L. D. Maestro, S. Ait-Si-Ali, The H3K9 methylation writer SETDB1 and its reader MPP8 cooperate to silence satellite DNA repeats in mouse embryonic stem cells. *Genes* **10**, 750 (2019).
46. D. L. Kwiatkowski, H. W. Thompson, D. C. Bloom, The polycomb group protein Bmi1 binds to the herpes simplex virus 1 latent genome and maintains repressive histone marks during latency. *J. Virol.* **83**, 8173–8181 (2009).
47. I. Müller *et al.*, MPP8 is essential for sustaining self-renewal of ground-state pluripotent stem cells. *Nat. Commun.* **12**, 3034 (2021).
48. M. C. Rodríguez, J. M. Dybas, J. Hughes, M. D. Weitzman, C. Boutell, The HSV-1 ubiquitin ligase ICP0: Modifying the cellular proteome to promote infection. *Virus Res.* **285**, 198015 (2020).
49. M. M. Gaidt *et al.*, Self-guarding of MORC3 enables virulence factor-triggered immunity. *Nature* **600**, 138–142 (2021), 10.1038/s41586-021-04054-5.
50. A. Hagelkruys *et al.*, The HUSH complex controls brain architecture and protocadherin fidelity. *Sci. Adv.* **8**, eabo7247 (2022).
51. S.-L. Tan *et al.*, Essential roles of the histone methyltransferase ESET in the epigenetic control of neural progenitor cells during development. *Development* **139**, 3806–3816 (2012).
52. J. S. Lee, P. Raja, D. M. Knipe, Herpesviral ICP0 protein promotes two waves of heterochromatin removal on an early viral promoter during lytic infection. *mBio* **7**, e02007 (2016).
53. M. Aubert *et al.*, Gene editing and elimination of latent herpes simplex virus in vivo. *Nat. Commun.* **11**, 4148 (2020).
54. M. Aubert *et al.*, Gene editing for latent herpes simplex virus infection reduces viral load and shedding in vivo. *Nat. Commun.* **15**, 4018 (2024).
55. G. Chougui, F. Margottin-Goguet, HUSH, a link between intrinsic immunity and HIV latency. *Front. Microbiol.* **10**, 224 (2019).
56. C. Badja *et al.*, Efficient and cost-effective generation of mature neurons from human induced pluripotent stem cells. *Stem Cells Trans. Med.* **3**, 1467–1472 (2014).
57. S. Cai, L. Han, Q. Ao, Y.-S. Chan, D.K.-Y. Shum, Human induced pluripotent cell-derived sensory neurons for fate commitment of bone marrow-derived schwann cells: Implications for remyelination therapy. *Stem Cells Trans. Med.* **6**, 369–381 (2017).
58. A. Corpet, P. Lomonte, ChIP-Seq dataset. Gene Expression Omnibus (GEO). https://www-ncbi-nlm-nih-gov.insb.bib.cnrs.fr/geo/query/acc.cgi?acc=GSE263436. Deposited 8 April 2024.